coatings

MDPI

Article

Influence of Bioactive Glass Addition on TC4 Laser Cladding Coatings: Microstructure and Electrochemical Properties

Yao Meng [1], Yuyun Yang [1,*], Changlin Zhang [2], Xiufang Cui [1,*], Erbao Liu [1], Guo Jin [1], Jiajie Kang [3,4] and Peng She [5,*]

[1] Department of Material Science and Chemical Engineering, Institute of Surface/Interface Science and Technology, Harbin Engineering University, Harbin 150001, China; mengyao@hrbeu.edu.cn (Y.M.); liuerbao@hrbeu.edu.cn (E.L.); jinguo@hrbeu.edu.cn (G.J.)
[2] Department of Gynecology, Pelvic Floor Disorders Center, The Seventh Affiliated Hospital of Sun Yat-sen University, Shenzhen 518107, China; zhangchanglin@sysush.com
[3] School of Engineering and Technology, China University of Geosciences, Beijing 100083, China; kangjiajie@cugb.edu.cn
[4] Zhengzhou Institute, China University of Geosciences (Beijing), Zhengzhou 450001, China
[5] Department of Orthopaedics, The Seventh Affiliated Hospital of Sun Yat-sen University, Shenzhen 518107, China
* Correspondence: yangyuyun@hrbeu.edu.cn (Y.Y.); cuixiufang@hrbeu.edu.cn (X.C.); shep@mail.sysu.edu.cn (P.S.)

Abstract: There is a growing interest in enhancing the bioactivity of TC4-based metallic biomaterials, which are known for their excellent biocompatibility. Bioactive glass (BG) has been recognized for its high potential in promoting bioactivity, particularly in osteo tissue engineering. This study focuses on investigating the influence of BG addition on the microstructure and electrochemical properties of TC4 coatings. The TC4/BG composite coatings were fabricated through laser cladding, and their microstructure was characterized using scanning electron microscopy (SEM) and X-ray diffraction (XRD). The electrochemical properties of the coatings were assessed through electrochemical impedance spectroscopy (EIS) and potentiodynamic polarization tests in three different solutions. The results revealed that the incorporation of BG had a significant impact on the microstructure of the TC4 coatings, leading to the formation of a well-defined interface between the TC4 matrix and the BG aggregates. The distribution of BG aggregates within the TC4 matrix coating was found to be random and unrelated to the specific regions of the coating. The metallographic microstructure variations were attributed to different heat dissipation conditions during the laser cladding process. Furthermore, the electrochemical corrosion behavior of TC4/BG composite coatings reveals that they exhibit stability similar to that of passive films and good resistance against media corrosion compared to TC4, while also showing enhanced corrosion resistance in 3.5 wt% NaCl and Dulbecco's modified Eagle medium (DMEM) solutions, indicating their potential for biomedical applications; however, the corrosion resistance decreases gradually in all solutions, potentially due to the elevated Cl^- concentration. Further research can explore bioactivity enhancement of TC4/BG composite coatings and investigate the long-term stability and biological response of these coatings in diverse physiological environments.

Keywords: laser cladding coatings; bioactive glass; microstructure; electrochemical properties

check for updates

Citation: Meng, Y.; Yang, Y.; Zhang, C.; Cui, X.; Liu, E.; Jin, G.; Kang, J.; She, P. Influence of Bioactive Glass Addition on TC4 Laser Cladding Coatings: Microstructure and Electrochemical Properties. *Coatings* **2023**, *13*, 1621. https://doi.org/10.3390/coatings13091621

Academic Editors: Narottam Bansal and Angela De Bonis

Received: 30 June 2023
Revised: 22 July 2023
Accepted: 1 August 2023
Published: 15 September 2023

Copyright: © 2023 by the authors. Licensee MDPI, Basel, Switzerland. This article is an open access article distributed under the terms and conditions of the Creative Commons Attribution (CC BY) license (https://creativecommons.org/licenses/by/4.0/).

1. Introduction

Ti-6Al-4V (TC4), a titanium alloy composed of titanium, aluminum, and vanadium, has garnered significant attention in various industries due to its exceptional mechanical properties, corrosion resistance, and widespread applications [1,2]. By comparison with other titanium alloys, such as Ti-3Al-8V-6Cr-4Mo-4Zr and Ti-3Al-2.5V (Grade 9), the excellent biocompatibility of titanium alloys has led to extensive research and applications

in the field of biomedical engineering, making it stand out compared to other titanium alloys [3,4]. TC4 exhibits a remarkable strength-to-weight ratio, excellent fatigue resistance, and exceptional corrosion resistance, making it a preferred choice in aerospace, automotive, and medical fields [2,5,6]. Corrosion resistance is another standout feature of TC4. It exhibits remarkable resistance to corrosion in various environments, including aggressive chemicals and physiological fluids [7,8]. This corrosion resistance is pivotal in applications where exposure to corrosive agents is inevitable, such as chemical processing plants, marine structures, and biomedical implants. In the medical field, TC4 is commonly employed in orthopedic implants, dental implants, and prosthetics due to its ability to withstand the corrosive nature of bodily fluids and provide long-term implant stability [9].

However, despite its numerous advantages, TC4 faces a limitation that hinders its utilization in biomedical applications: its lack of bioactivity [9]. In the context of medical implants, bioactivity refers to the ability of a material to bond with living tissues, promote cell adhesion, and stimulate tissue regeneration. TC4 exhibits excellent biocompatibility and has been clinically applied in terms of medical devices, implants, and tissue-engineered products [10]; however, its inert nature prevents direct interaction with biological systems, limiting its ability to facilitate osseointegration and tissue regeneration [11]. As a result, there is a growing demand for research to develop strategies that can enhance the bioactivity of TC4 [9,11,12], thereby expanding its applications in the biomedical field.

Addressing the lack of bioactivity in TC4 holds significant promise for advancements in medical implants and prosthetics. By enhancing TC4's bioactivity, it becomes possible to promote better integration with host tissues, reduce the risk of implant rejection, and enhance the long-term stability of implants. Achieving bioactivity in TC4 could involve various approaches, such as surface modification techniques [6,9,13], the addition of bioactive coatings [14–17], or the incorporation of bioactive elements such as bioactive glass (BG) [18–21]. Further research is essential to investigate these strategies and unlock the full potential of TC4 in biomedical applications.

BG has emerged as a remarkable material in the field of biomedical engineering due to its inherent bioactivity and exceptional tissue regeneration properties. BG possesses the unique ability to form a biologically active hydroxyapatite layer on its surface when exposed to bodily fluids [22,23], making it highly attractive for various biomedical applications. This introduction aims to highlight the significance of BG and its potential benefits when incorporated into TC4, a titanium alloy, to impart bioactivity and enhance its performance in biomedical applications, while preserving its electrochemical properties.

Therefore, the addition of BG to TC4 potentially enhances its corrosion resistance, and further extending its lifespan and performance can be achieved in biomedical applications. The unique composition of BG and its ability to form a protective hydroxyapatite layer can act as a barrier against corrosive agents present in the physiological environment. This corrosion-resistance property is of utmost importance in maintaining the structural integrity and functionality of biomedical implants over an extended period.

Fabrication methods play a crucial role in the development and production of advanced materials with tailored properties. In the context of TC4/BG composite coatings, the laser cladding method has emerged as a suitable technique for depositing these coatings. Laser cladding is a sophisticated additive manufacturing technique that involves the deposition of material onto a substrate using a high-energy laser beam [15,24]. One of the key advantages of laser cladding is its ability to provide precise control over the composition of the deposited coating. By adjusting the laser parameters and controlling the powder feed rate, it is possible to achieve the desired composition and distribution of TC4 and BG phases in the coating. This level of control allows for the customization of coating properties to meet specific requirements, such as enhanced bioactivity, mechanical strength, or corrosion resistance. Furthermore, laser cladding exhibits a minimal heat-affected zone (HAZ) compared to other fabrication methods. The localized heating provided by the laser beam allows for precise melting and solidification of the coating material, minimizing the thermal impact on the substrate [25]. In addition to precise control over composition and

the minimal HAZ, laser cladding also offers excellent bonding between the coating and the substrate. The high-energy laser beam melts both the coating material and the substrate, promoting metallurgical bonding between the two [26]. This strong bonding ensures good adhesion, mechanical stability, and efficient load transfer between the coating and the substrate. The robust bonding interface is essential for the longevity and performance of TC4/BG composite coatings, especially in demanding applications where mechanical stresses and environmental factors come into play.

In recent studies, laser cladding technology has been reported for the preparation of BG coatings on titanium alloy surfaces [27–29]. Although the overall reactivity of the coating increases due to the addition of BG on the entire surface of the titanium alloy through laser cladding, it is important to note that BG is a non-metallic material with completely different properties from the metallic titanium alloy substrate. Therefore, they cannot form metallurgical compounds and their bonding remains a physical embedding connection. As the service life of the implant increases, there is a risk of detachment and delamination of the BG coating from the titanium alloy substrate after degradation, which can lead to the detachment of previously adhered cells and other entities growing on the BG coating.

In this study, to avoid such detachment issues, we designed a coating that consists of both BG and TC4 (titanium alloy) coated on the TC4 substrate using laser cladding technology. The molten TC4 and partially molten or non-melted BG aggregates were coated onto the TC4 substrate, and the randomly distributed BG aggregates within the coating not only provided good bioactivity to TC4, enhancing cell adhesion and differentiation, but also did not pose a risk of cells' detachment due to their random distribution within the coating. Therefore, this research aims to contribute to the field by employing the laser cladding method to fabricate TC4/BG composite coatings. The investigation focuses on evaluating the effects of incorporating BG on TC4, and assessing the resulting microstructure, chemical composition, and corrosion resistance of the developed TC4/BG composites.

2. Materials and Methods

2.1. Materials

The TC4 substrate utilized in this experimental study was sourced from Baoji Rongsheng Titanium Industry Co., Ltd. (Baoji, China). The chemical composition of the TC4 substrate is presented in Table 1. The cladding materials employed in the study include TC4 powder and BG powder. The TC4 powder, obtained from Jiangsu Jinwu New Material Co., Ltd. (Taizhou, China), possesses a particle size D_{10} of 41.4 μm, and its chemical composition is illustrated in Table 2. The BG powder was synthesized in the laboratory using the sol–gel method, and its chemical composition is outlined in Table 3. The synthesis process involved pouring a solution containing 3 mL of tetraethyl orthosilicate (TEOS, >99%) and 25 mL of ethanol into another solution consisting of 4.5 mL of ammonium hydroxide (28%), 10 mL of ethanol, and 15 mL of deionized water under continuous stirring. After allowing the mixture to react for 30 min, proportional calcium nitrate tetrahydrate (99%) was added. The suspension was stirred for an additional 90 min before being centrifuged at 7830 rpm for 5 min to collect the deposits. The collected deposits were washed twice with water and once with ethanol, followed by drying at 60 °C for 6 h. Subsequently, the deposits were subjected to calcination at 700 °C for 2 h with a heating rate of 2 °C/min. All chemicals used in the synthesis were purchased from Sigma-Aldrich (St. Louis, MO, USA) and used without further purification.

Table 1. Chemical composition of TC4 alloy substrates.

Elements	Al	V	Fe	C	N	H	O	Ti
Wt%	6.1~6.09	4.1~3.9	0.12~0.11	0.01~0.009	0.001	0.012~0.002	0.147~0.13	Bal.

Table 2. Chemical composition of TC4 powders.

Elements	Al	V	Fe	C	N	H	O	Ti
wt%	6.36	4.01	0.180	0.01	0.01	0.002	0.10	Bal.

Table 3. Composition of BG powders.

Composites	CaO	SiO_2	P_2O_5
wt%	49	45	6

2.2. Coating Preparation

Quantities of 83 wt% TC4 powders and 17 wt% BG powders were accurately weighed and subsequently subjected to a drying process in a designated drying oven. The TC4 and BG powders, once dried, were mechanically blended together to form a homogenous mixture. This mixture was then applied as a pre-coating on the TC4 substrate, resulting in a coating thickness of approximately 2 mm.

The samples were prepared utilizing a YLS-3000 laser system manufactured by IPG company (Harbin, China). After the optimization of the process, the following parameters were selected for the experiment: a laser power of P = 2000 W, a scanning speed of V = 10 mm/s, a spot diameter of D = 3 mm, and a gun head height of 4 cm. A total of 8 passes were performed with a pass overlap rate of 30%.

2.3. Characterization Methods

The XPert-Pro automated X-ray diffractometer (manufactured by Philips, MRD 3055, Amsterdam, The Netherlands) was employed to analyze the phase composition of the TC4 substrate, TC4/BG coating surface, and BG powder. The X-ray source used was a Co target (0.17897 mm), and the scanning range was set from 10° to 80° with a scanning speed of 10°/min. The QUANTA 200 environmental scanning electron microscope (manufactured by FEI, Quanta 250, Hillsboro, OR, USA) equipped with an energy-dispersive spectroscopy (EDS) system was utilized to observe the microstructure and elemental distribution of the cross-section of the TC4/BG coating samples. The 4XC-BD metallographic microscope (manufactured by Shanghai Optical Instrument Factory, Shanghai, China) was employed to observe the cross-section microstructure of TC4/BG coating samples.

Electrochemical experiments were conducted using a CHI660E electrochemical workstation (manufactured by Shanghai Chenhua Instrument Co., Ltd., Shanghai, China) with a three-electrode system. The working electrode was either the TC4 substrate or the TC4/BG coating sample (with the working area calculated using ImageJ software bundled with 64-bit Java 8), sealed with dental putty, while the reference electrode was a saturated calomel electrode. Platinum foil was used as the auxiliary electrode. The electrolyte solution consisted of a 3.5 wt% NaCl solution, Hank's balanced salt solution, and Dulbecco's modified Eagle medium (DMEM) solution (Hank's solution (with the main composition listed in Table 4) and DMEM solution (with the main composition listed in Table 5) were produced by Shanghai Macklin Biochemical Co., Ltd., Shanghai, China). Open circuit potential (OCP) testing was conducted for 300 s to stabilize the testing system. Electrochemical impedance spectroscopy (EIS) was performed within a frequency range of 10^{-2} Hz to 10^5 Hz, with an AC amplitude of 10 mV. Nyquist plots and Bode plots were used to describe the corrosion behavior, and the ZSimpWin software 3.0 was utilized to fit and process the EIS data. Potentiodynamic polarization scans were conducted within a potential range of −500 mV vs. OCP to 3.5 V, at a scan rate of 1 mV/s. The Tafel extrapolation method was employed to analyze the polarization curves.

Table 4. Composition of Hank's equilibrium salt solution.

Composition	NaCl	KCl	$CaCl_2$	$NaHCO_3$	$NaH_2PO_4 \cdot 2H_2O$	$MgCl_2 \cdot 6H_2O$	KH_2PO_4
Concertation (g/L)	8.0	0.4	0.14	0.35	0.06	0.10	0.6

Table 5. Composition of DMEM solution.

Composition	NaCl	KCl	$CaCl_2$	$NaHCO_3$	NaH_2PO_4 (Anhydrous)	$MgSO_4$ (Anhydrous)	Amino Acids	D-Glucose
Concertation (g/L)	6.4	0.4	0.2	3.7	0.109	0.09767	1.60539	4.5

3. Results and Discussion

3.1. Composition and Microstructure of Composite Coatings

Figure 1 presents the X-ray diffraction (XRD) patterns of the TC4 substrate, BG powder, and TC4/BG composite coating. The XRD patterns clearly demonstrate a substantial overlap between the TC4/BG and BG phases in the range of 10° to 25°, indicating the presence of BG in the TC4/BG coating with relatively low crystallinity. Notably, distinctive peaks are observed in the 15° to 25° range, providing further evidence of the BG phase's existence within the composite coating. The appearance of these characteristic peaks in the XRD pattern confirms the incorporation of BG in the TC4/BG composite.

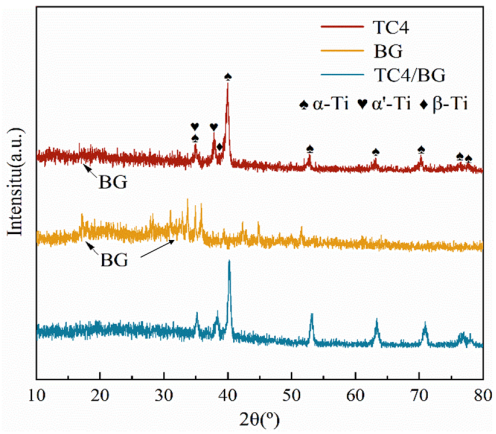


Figure 1. XRD patterns of TC4/BG, TC4, and BG.

Additionally, within the 30–40° range, BG exhibits certain peaks corresponding to low crystallinity, which can be attributed to the specific BG preparation process and composition. This observation aligns with findings from the related literature, where similar low crystallinity peaks have been reported under similar conditions [30]. However, it is important to note that in the XRD pattern of the TC4/BG composite coating, the presence of highly crystalline titanium alloy peaks in this range masks the distinct BG peaks. Consequently, the presence of BG in the composite coating may not be as easily discernible within this specific range.

Further detailed analysis utilizing Jade software reveals that the TC4/BG composite coating mainly consists of characteristic peaks corresponding to α-Ti, β-Ti, and α′-Ti phases. These peaks exhibit higher crystallinity and relatively strong peak intensities, which align with the typical characteristic peaks of TC4 (composed mainly of α-Ti and β-Ti phases). The appearance of the α′-Ti phase in the TC4/BG composite is believed to be a result of the rapid cooling experienced during the solidification process, as reported in previous studies [24]. Based on the comprehensive XRD results, the primary composition identified within the TC4/BG coating includes α-Ti, β-Ti, α′-Ti, and BG phases.

Figure 2a displays SEM images of the TC4/BG composite coating. The clustered particles seen in the recesses of Figure 2 correspond to BG, while the remaining regions

represent TC4. BG is present in TC4 as clustered particles, as illustrated in Figure 2a, which highlights that BG particles are either fully exposed or partially covered by TC4. A clear interface can be observed between BG and TC4. Rather than forming a multi-component homogeneous system, the coating constitutes a composite material composed of TC4 and BG. Hence, it can be inferred that the coating is referred to as the TC4/BG composite coating. Moreover, the presence of micro-sized cracks near the BG particles within the coating is evident, which can be attributed to the internal stresses induced by the differential shrinkage ratio during the cooling process. These cracks have the potential to compromise the integrity and performance of the TC4/BG composite coatings.

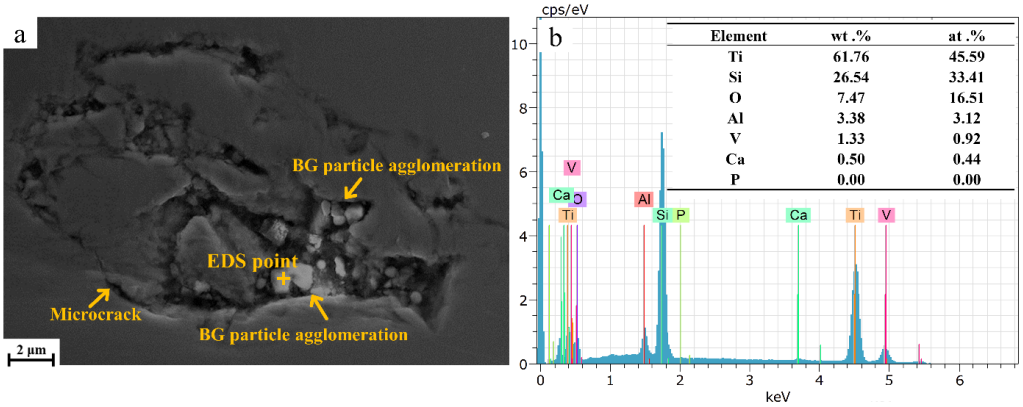


Figure 2. SEM image (**a**) of TC4/BG composite coatings and EDS (**b**) of BG clusters embedded within TC4/BG composite coating.

Figure 2b shows the results of EDS analysis, which was conducted on the TC4/BG composite coating to identify the presence of BG particles embedded within the TC4 matrix. EDS point analysis was performed on the clustered particles of BG within the TC4/BG composite. The analysis confirmed the presence of BG particles based on the detection of Si, Ca, and O elements, which are characteristic constituents of BG. This analysis conclusively identified the clustered particles containing Si and Ca elements as BG within the TC4/BG composite. Additionally, the elements Ti, Al, and V originate from the matrix phase of TC4.

In order to accurately characterize the metallurgical features of different regions within the TC4/BG composite coating, a detailed analysis of the microstructural morphology was conducted.

Figure 3 presents the metallographic morphology images of various regions within the TC4 matrix phase in the TC4/BG composite coating. It can be observed from Figure 3 that the cladding layer exhibits a defect-free microstructure, devoid of cracks and pores. Furthermore, due to inherent microstructural variations, the cladding layer can be classified into three distinct regions: the top region (Figure 3A,a), the middle region (Figure 3B,b), and the bottom region (Figure 3C,c). In the top region of the coating, TC4 demonstrates a fine-grained equiaxed structure with high density. The fine-grained nature of the microstructure indicates that the individual grains are relatively small in size and have a more uniform distribution. Moreover, the fine-grained equiaxed structure enhances the homogeneity of the material, leading to a more uniform distribution of properties throughout the top region. Equiaxed grains refer to grains that have similar dimensions in all three directions, resulting in a more isotropic material behavior. The presence of a fine-grained equiaxed structure in this region is often associated with rapid solidification during the laser cladding process. As the molten TC4 material is rapidly deposited onto the substrate, it experiences rapid cooling, leading to the formation of small and evenly distributed grains. This rapid cooling prevents significant grain growth and promotes the formation of a dense and compact microstructure. The high density of grains in the top region of the coating contributes to improved mechanical properties and enhanced performance.

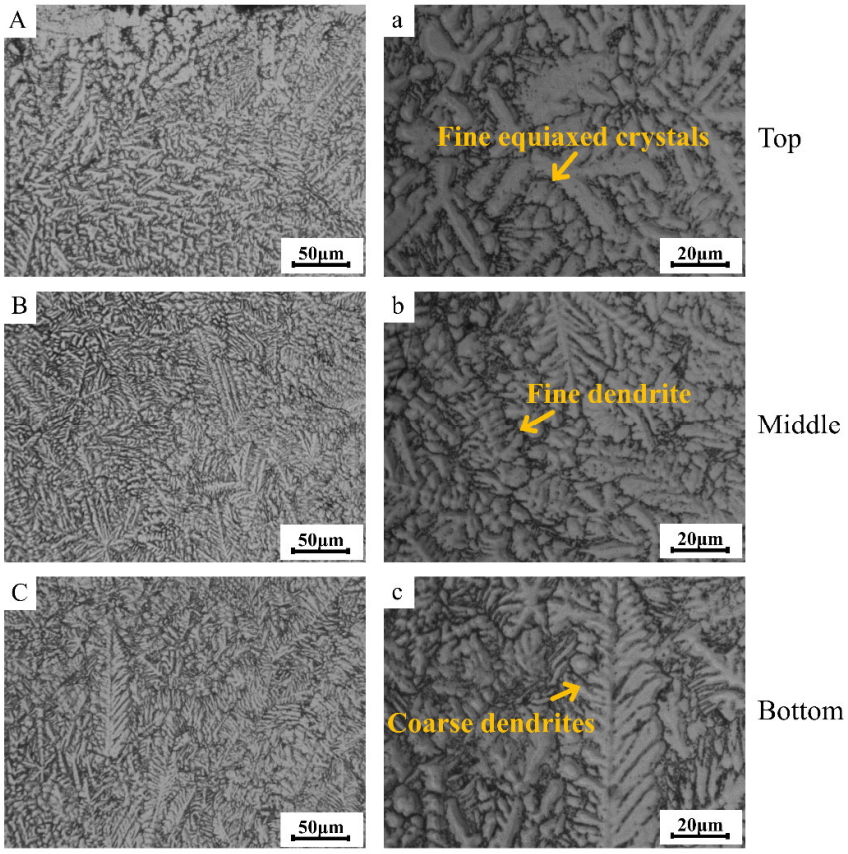


Figure 3. Metallographic images of different regions (top region (**A**,**a**), middle region (**B**,**b**) and bottom region (**C**,**c**) of coating) of the TC4 matrix phase within the TC4/BG composite coating.

Moving towards the middle region, TC4 exhibits relatively smaller dendritic grains. Dendritic grains are characterized by a tree-like or branching structure that forms during the solidification process of the material. In this region, the microstructure undergoes some changes compared to the top region, resulting in the formation of smaller and more intricately shaped grains. The presence of smaller dendritic grains in the middle region is influenced by the thermal history experienced during the laser cladding process. As the molten TC4 material is deposited onto the substrate and solidifies, the cooling rate in this region is slightly slower than that in the top region. This moderate cooling rate allows the material to form dendritic structures, where the solidification front branches out and creates smaller grain structures. The smaller dendritic grains in this region may provide some benefits to the overall properties of the cladding layer. Furthermore, the presence of smaller dendritic grains may offer some advantages in terms of microstructural stability. However, it is essential to note that the presence of smaller dendritic grains in the middle region is not entirely uniform and can vary in distribution and orientation. The exact characteristics of the microstructure in this region may depend on various process parameters, including laser power, scanning speed, and powder feed rate.

Finally, in the bottom region of the coating (Figure 3C,c), TC4 reveals coarser dendritic grains. Coarse dendritic grains exhibit a more pronounced and larger branching structure compared to the smaller dendritic grains observed in the middle region. The transition to coarser grains in this lower part of the cladding layer is a result of the distinct thermal conditions experienced during the laser cladding process. As the molten TC4 material is deposited and solidifies in the bottom region, the cooling rate is further reduced compared to both the middle and top regions. The slower cooling rate in this area allows for the growth of larger dendritic grains, which tend to form with extended solidification times. The presence of coarser dendritic grains in the bottom region can have significant implications

for the microstructure and properties of the cladding layer. The increased size of these dendrites results in a reduction in the overall grain boundary density.

The transition in the grain size of TC4 within the cladding layer, ranging from fine to coarse, can be attributed to the heterogeneous heat dissipation conditions prevailing in different segments of the laser cladding process.

The distinctive metallographic morphology observed is primarily associated with the laser cladding preparation process. During cladding, the heat dissipation within the coating primarily occurs through the substrate, resulting in a decreasing temperature gradient (G) from the bottom to the top of the cladding layer. Concurrently, the solidification rate (R) increases from the bottom to the top. According to the constitutional undercooling theory, the G/R ratio governs the crystal growth morphology, with lower G/R values favoring dendritic growth and extremely low G/R values leading to equiaxed growth.

At the bottom of the coating, the G/R value is relatively low, promoting dendritic growth. The longer solidification time due to the lower R value results in the formation of coarser dendritic structures [31]. In the middle region of the coating, the decrease in G and increase in R lead to a lower G/R ratio, causing shorter and denser secondary dendritic branching. Additionally, the increased R value contributes to the development of finer dendritic structures, yielding a microstructure characterized by relatively smaller dendritic grains.

At the top of the coating, the G/R value further decreases, leading to the formation of a significantly high degree of constitutional undercooling in the liquid phase region at the solidification interface. This creates a highly undercooled composition range, promoting heterogeneous nucleation. Furthermore, the laser beam may serve as a stirring mechanism, promoting fragmentation of dendritic structures. The top region exhibits numerous independent crystals growing freely within the highly undercooled melt, resulting in the formation of fine-grained equiaxed structures with varying growth directions but comparable dimensions. Additionally, the higher R value in this region contributes to the formation of a dense microstructure consisting of fine equiaxed grains, as shown in Figure 3A,a.

Figure 4 depicts the metallographic images of the distribution of BG aggregates in different regions of the TC4/BG composite coating. The BG clusters are randomly distributed throughout the coating, from the top to the bottom. The size of the BG aggregates within the composite coating is likely influenced by the aggregation state of BG during the powder mixing process. Therefore, the size of BG aggregates appears to be random and unrelated to their distribution within the coating regions.

3.2. Electrochemical Behavior of TC4/BG Composite Coatings

The primary aim of this study was to examine the effects of incorporating BG into TC4 laser cladding coatings, with a specific focus on evaluating its influence on the electrochemical corrosion behavior. Furthermore, our objective was to verify that the addition of BG can enhance the bioactivity of TC4 coatings while preserving their electrochemical corrosion-resistance properties. Subsequent investigations will delve deeper into the exploration of the bioactivity aspects, aiming to further elucidate the impact of BG on TC4 coatings and their potential biomedical applications. This study mainly focuses on the electrochemical behaviors of TC4/BG composite coatings.

In this study, 3.5 wt% NaCl, Hank's, and DMEM solutions were used as electrolytes in the electrochemical experiments to investigate the differences in the electrochemical behavior of the composite coating in different physiological solutions.

Figure 5 shows the potentiodynamic polarization curves of TC4 substrate and TC4/BG coating in 3.5 wt% NaCl, Hank's, and DMEM solutions. In all three solutions, both TC4/BG and TC4 exhibited distinct passive regions in their polarization curves, but with slight differences in the passivation behavior. By considering the passivation current density values in Table 6, it can be observed that TC4/BG and TC4 have different passivation current density (I_{pp}) values in different solutions, but they are both in the magnitude of 10^{-6} A·cm^{-2}. This indicates that TC4/BG and TC4 exhibit similar stability of the

passive film formed by the externally applied anodic current in the same solution, and the comparable I_{pp} values suggest that both coatings have good resistance against media corrosion [32,33].

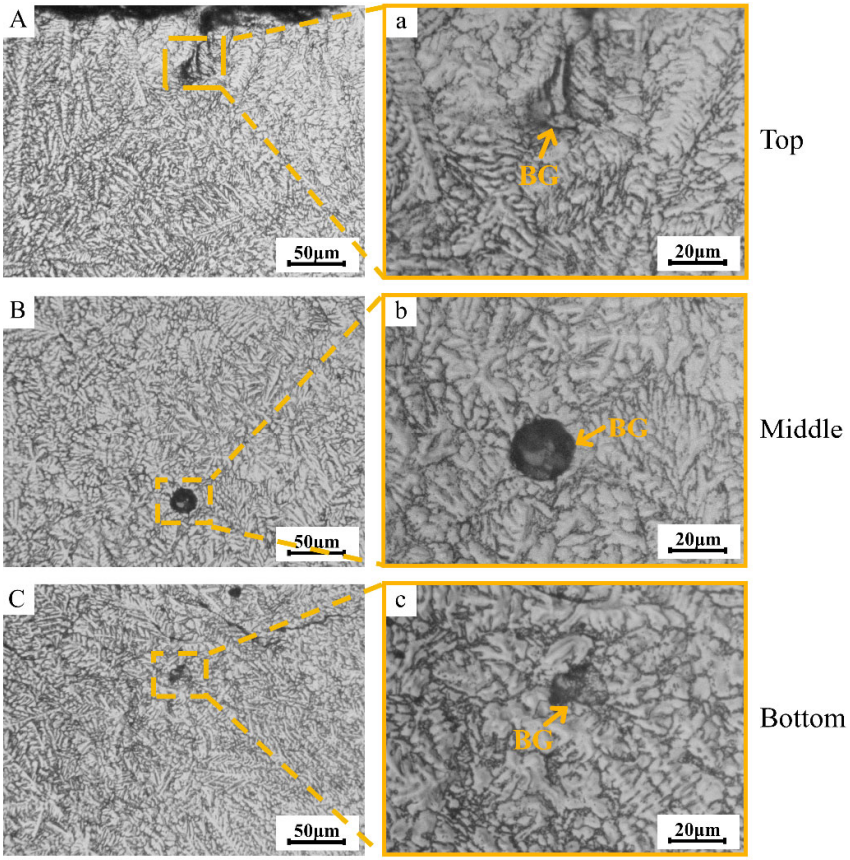


Figure 4. Metallographic images of different regions (top region (**A**,**a**), middle region (**B**,**b**) and bottom region (**C**,**c**) of coating) of BG clusters' distribution within the TC4/BG composite coating.

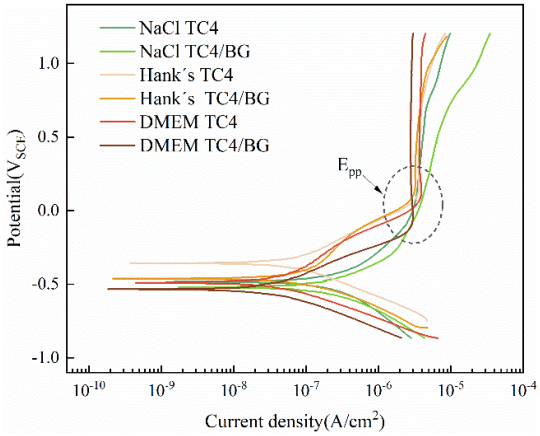


Figure 5. Polarization curves of TC4/BG coating and TC4 substrate in DMEM, Hank's, and 3.5 wt% NaCl solutions.

Table 6. Fitting data of polarization curves for TC4/BG coating and TC4 substrate.

	E_{corr}/V_{SCE}	$I_{corr}/(A \cdot cm^{-2})$	E_{pp}/V_{SCE}	$I_{pp}/(A \cdot cm^{-2})$
NaCl TC4	−0.487	1.37×10^{-7}	−0.005	2.96×10^{-6}
Hank's TC4	−0.360	5.72×10^{-8}	0.110	3.51×10^{-6}
DMEM TC4	−0.495	3.44×10^{-8}	0.252	3.77×10^{-6}
NaCl TC4/BG	−0.513	1.15×10^{-7}	−0.023	3.41×10^{-6}
Hank's TC4/BG	−0.459	5.71×10^{-8}	0.143	3.20×10^{-6}
DMEM TC4/BG	−0.532	2.61×10^{-8}	0.126	2.87×10^{-6}

Furthermore, TC4/BG coating shows different resistance to the solution erosion caused by anodic polarization in the three solutions, although the differences are not significant. TC4 exhibits a trend similar to that of TC4/BG coatings in its electrochemical behavior. The corrosion resistance of samples is often evaluated by the magnitude of corrosion current density, where a lower corrosion current density (I_{corr}) corresponds to higher corrosion resistance. As shown in Table 6, in 3.5 wt% NaCl and DMEM solutions, TC4/BG exhibits better corrosion resistance compared to TC4, but the difference is not significant. In Hank's solution, TC4/BG and TC4 exhibit comparable corrosion resistance. Additionally, both TC4/BG and TC4 demonstrate excellent corrosion resistance in the three solutions, with I_{corr} values having a maximum magnitude of 10^{-7} A·cm^{-2}. During the electrochemical process, passivation behavior refers to the formation of a stable passive film on the surface of titanium alloy induced by electrochemical anodic oxidation. This passive film serves as a protective barrier, effectively inhibiting the continuation of corrosion [34,35]. In the three solutions, both TC4/BG and TC4 exhibit a decreasing trend in corrosion resistance, with the order of DMEM < Hank's < 3.5 wt% NaCl solution. Taking into account the composition of the three solutions, it is worth noting that only the DMEM culture medium contains organic substances, but without corrosive organic compounds [36]. The primary inorganic salt constituents in these solutions consist of Na^+ and Cl^-, and their concentrations increase in the order of DMEM, Hank's, and 3.5 wt% NaCl solutions. The literature has reported a correlation between the increased Cl− concentration in the solution and a decrease in the corrosion resistance of titanium alloys [37,38]. Hence, the disparity in corrosion resistance between TC4/BG and TC4 in the three solutions can be attributed to the elevated Cl− concentration, resulting in diminished corrosion resistance.

EIS results of TC4/BG coating and TC4 substrate in three different solutions are presented through Nyquist and Bode plots, as illustrated in Figure 6. As shown in Figure 6a, both TC4/BG and TC4 display a single semicircular capacitive impedance arc in their Nyquist plots, indicating that their EIS profiles consist of a single time constant [39]. However, the Nyquist plots of TC4/BG and TC4 differ in terms of the radius of the capacitive impedance arc. Generally, a larger arc signifies higher corrosion resistance of the samples [40]. Hence, in 3.5 wt% NaCl and DMEM solutions, TC4/BG exhibits superior corrosion resistance compared to TC4. Conversely, in Hank's solution, TC4/BG demonstrates slightly poorer corrosion resistance than TC4.

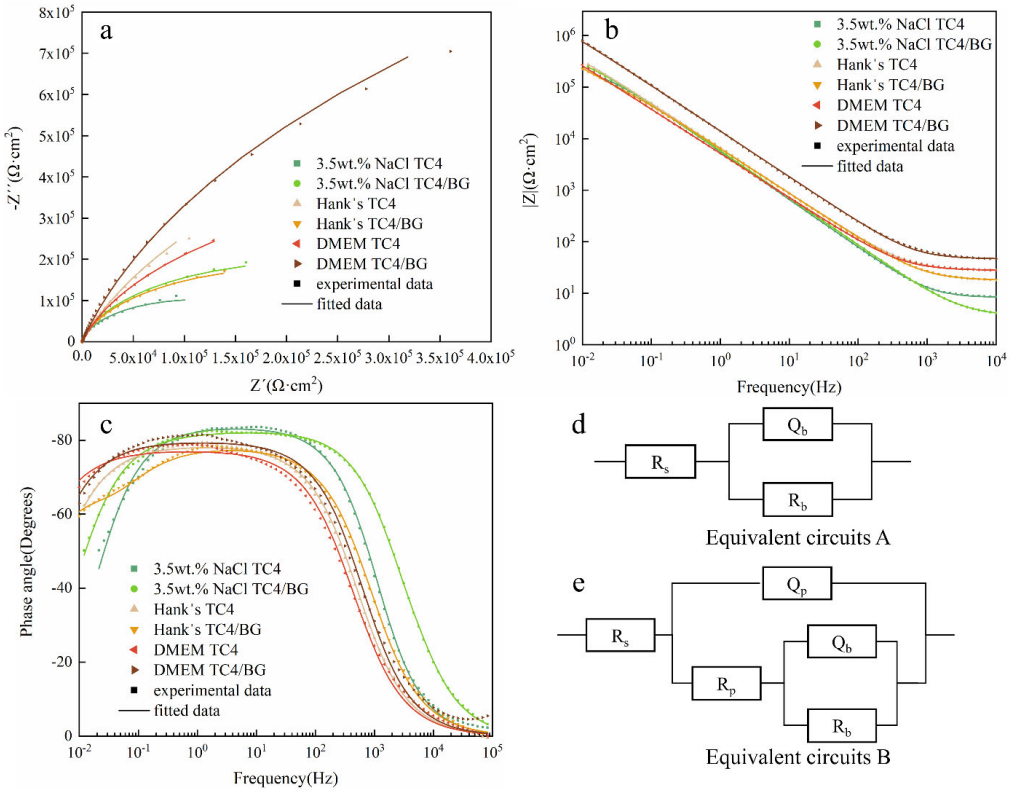


Figure 6. Nyquist (**a**) and Bode (**b**,**c**) plots of TC4/BG coatings and TC4 substrates. Equivalent circuit models (**d**) and (**e**) to fit electrochemical impedance spectroscopy (EIS) of TC4 substrate and TC4/BG coating.

As shown in Figure 6b,c, the Bode modulus curves of TC4 and TC4/BG display a linear slope with an approximate value of −1 at the mid-to-low-frequency range. The phase angles approach −90° from the mid-frequency to the low-frequency region, indicating the presence of dense passive films on the surface of both samples [41–43]. In the Bode impedance plot (Figure 6b), at low frequencies, the TC4/BG impedance modulus ($|Z|_{0.01Hz}$) is higher compared to that of TC4 in 3.5 wt% NaCl and DMEM solutions. However, in Hank's solution, TC4/BG exhibits a slightly lower $|Z|_{0.01Hz}$ compared to TC4. Additionally, in 3.5 wt% NaCl and Hank's solutions, both TC4/BG and TC4 show comparable $|Z|_{0.01Hz}$ values.

In the Bode phase angle plot (Figure 6c), a distinct peak can be observed in the phase angle–lgf curve of TC4/BG and TC4 at frequencies where the phase angle approaches −80° in the mid-to-low-frequency range. Comparing the flat regions of the peaks, it is evident that in DMEM, the flat region of TC4/BG exhibits a higher phase angle than TC4. Conversely, in 3.5 wt% NaCl and Hank's solutions, the flat region of TC4/BG shows a slightly lower phase angle compared to TC4 (opposite trend). However, there is no significant difference in the phase angle between TC4/BG and TC4 in all three solutions.

It is well-established that higher impedance and phase angle values indicate better corrosion resistance of the samples [44]. Based on the Bode plots, it can be inferred that TC4/BG demonstrates corrosion resistance similar to that of TC4 in 3.5 wt% NaCl solution, slightly lower corrosion resistance than that of TC4 in Hank's solution, and slightly stronger corrosion resistance than that of TC4 in DMEM solution.

Equivalent circuits A and B, as depicted in Figure 6d,e, respectively, were utilized to fit EIS data of TC4 and TC4/BG [41–43]. Table 7 presents the interpretation of the equivalent components depicted in Figure 6d,e. The table provides a comprehensive understanding of the meaning and significance of each component in the respective equivalent circuits. Circuit A is commonly associated with materials that possess a dense passive film on the surface, serving as a robust barrier against electrolyte corrosion and reducing the material's corrosion rate, as observed in TC4. Conversely, circuit B represents an alternative equivalent

circuit composed of a dense blocking layer and a porous layer, effectively mitigating the corrosion rate, as evidenced in TC4/BG.

Table 7. Equivalent components in the circuit.

Equivalent Component	Meaning
R_s	Electrolyte resistance
R_p	Charge transfer resistance of the porous layer
Q_p	Constant phase angle element of the porous layer
R_b	Charge transfer resistance of the dense barrier layer
Q_b	Constant phase angle element of the dense barrier layer

In atmospheric environments, titanium alloys, including TC4, naturally form a dense passive film mainly composed of TiO_2 on their surfaces. However, in the case of TC4/BG coatings, the presence of microcracks resulting from the detachment of the BG layer compromises the integrity of the surface passivation film. Thus, the analysis of TC4/BG EIS using circuit B provides valuable insights into the surface structure and behavior of the coating.

Furthermore, the characteristic shape of the Nyquist plots, exhibiting only a capacitive arc without an inductive arc, indicates that the selected equivalent circuit for fitting the EIS should not include an inductance element. Therefore, the chosen equivalent circuit in this study aligns with this observation.

In the two models mentioned above, R_p and R_b represent charge transfer resistances with units of $\Omega \cdot cm^2$. A higher charge transfer resistance indicates greater hindrance of electrochemical reactions, implying better corrosion resistance of the electrode material in the solution. Q_p and Q_b are constant phase angle elements. In complex corrosion processes involving interfaces, the capacitance in impedance spectra is typically non-ideal and exhibits deviations. To address this, a constant phase angle element (CPE) is used as a substitute for capacitance, denoted as Q. The impedance of Q is defined as $Z_Q = [Y_0(j\omega)^n]^{-1}$. Therefore, the equivalent element Q has two parameters: Y_0, measured in $\Omega^{-1} \cdot cm^{-2} \cdot s^{-n}$, and n, a dimensionless exponent ranging between 0 and 1.

The fitting parameters are listed in Table 8. The quality of the fit was assessed using the chi-square (χ^2) value, and both TC4 and TC4/BG exhibited χ^2 values on the order of 10^{-4}, indicating a good fit quality. It is noteworthy that the EIS of TC4/BG suggests that the equivalent circuit should consist of only one time constant. However, the selected equivalent circuit, based on the analysis of the sample's surface structure and references, incorporates two time constants, and the fitting results align closely with the actual measurement data. The presence of a single time constant in the EIS of TC4/BG, despite its dual-layer film structure, can be attributed to the following reason: the porous layer appears to be sufficiently thin and exhibits low resistance compared to the blocking layer, thus making a negligible contribution to the electrochemical performance [45]. This observation is supported by the significant difference in magnitude between R_b and R_p in TC4/BG (three orders of magnitude apart). Therefore, the electrochemical behavior of TC4/BG is primarily governed by the blocking layer, resulting in the EIS displaying a single time constant.

As shown in Table 8, the value of R_p in TC4/BG is significantly smaller than R_b, with a difference of at least three orders of magnitude. Therefore, R_p can be considered negligible when evaluating the charge transfer resistance [46]. In both 3.5 wt% NaCl and DMEM solutions, TC4/BG exhibits a larger R_b compared to TC4, indicating superior corrosion resistance for TC4/BG. However, in Hank's solution, the R_b of TC4/BG is slightly smaller than that of TC4, suggesting slightly inferior corrosion resistance of TC4/BG in this particular environment. Furthermore, it is noteworthy that the R_b values for both TC4/BG and TC4 decrease in DMEM, Hank's, and 3.5 wt% NaCl solutions, indicating a gradual decrease in corrosion resistance. This trend is consistent with the polarization

curve results and can be attributed to the detrimental effect of increased Cl^- concentration on the corrosion resistance of the materials.

Table 8. Fitting results of EIS for TC4/BG coating and TC4 substrate.

	R_s ($\Omega \cdot cm^2$)	Q_p-Y_0 ($\Omega^{-1} \cdot cm^{-2} \cdot s^{-n}$)	Q_p-n	R_p ($\Omega \cdot cm^2$)	Q_b-Y_0 ($\Omega^{-1} \cdot cm^{-2} \cdot s^{-n}$)	Q_b-n	R_b ($\Omega \cdot cm^2$)	χ^2
NaCl TC4	8.27	—	—	—	$32.3 \times 10-5$	0.929	2.41×10^5	$9.76 \times 10-4$
Hank's TC4	27.7	—	—	—	$3.09 \times 10-5$	0.873	9.56×10^5	$3.98 \times 10-4$
DMEM TC4	27.7	—	—	—	$3.98 \times 10-5$	0.859	1.79×10^6	$1.37 \times 10-3$
NaCl TC4/BG	3.63	$1.89 \times 10-5$	0.929	123.2	$1.35 \times 10-5$	0.852	4.51×10^5	$2.33 \times 10-4$
Hank's TC4/BG	17.8	$3.17 \times 10-5$	0.868	238.6	$2.08 \times 10-5$	0.821	9.47×10^5	$4.45 \times 10-4$
DMEM TC4/BG	46.3	$1.43 \times 10-5$	0.885	952.3	$4.65 \times 10-5$	0.999	2.06×10^6	$2.70 \times 10-3$

TC4/BG coating exhibits excellent corrosion resistance in all three solutions. In 3.5 wt% NaCl and Hank's solutions, TC4/BG shows comparable corrosion resistance to that of TC4, while in DMEM, TC4/BG demonstrates slightly superior corrosion resistance compared to that of TC4. The passivation behavior of TC4/BG and TC4 also exhibits slight differences, with both materials forming stable surface passivation films under anodic polarization, albeit with minor variations. Additionally, the corrosion resistance of both TC4/BG and TC4 gradually decreases in DMEM, Hank's, and 3.5 wt% NaCl solutions. The ability of the passivation films formed under anodic polarization to withstand solution attack varies between TC4/BG and TC4, although no significant disparity is observed.

4. Conclusions

In conclusion, the investigation of TC4/BG composite coatings revealed valuable insights into their microstructural morphology and electrochemical behavior. The XRD analysis confirmed the presence of α-Ti, β-Ti, α′-Ti, and BG phases in the TC4/BG coating, indicating its composite nature. SEM and EDS analyses provided visual evidence of the distribution and composition of BG clusters within the TC4 matrix. The presence of micro-sized cracks near the BG particles indicated the presence of internal stresses induced by differential shrinkage during the cooling process. The metallographic analysis of the TC4 matrix phase within the coating unveiled distinct regions with varying grain sizes, attributed to heterogeneous heat dissipation conditions during laser cladding. The top region exhibited a fine-grained equiaxed structure, the middle region showed smaller dendritic grains, and the bottom region displayed coarser dendritic grains. These variations in grain size were influenced by the temperature gradient and solidification rate during the cladding process.

The electrochemical behavior of TC4/BG composite coatings was evaluated in different physiological solutions. The potentiodynamic polarization curves indicated that both TC4/BG and TC4 coatings formed stable passive films, exhibiting good resistance against corrosion. TC4/BG exhibited slightly better corrosion resistance than that of TC4 in 3.5 wt% NaCl and DMEM solutions, while their corrosion resistance was comparable in Hank's solution. The EIS analysis further supported these findings, showing larger capacitive impedance arcs and higher impedance modulus values for TC4/BG in 3.5 wt% NaCl and DMEM solutions. The interpretation of the equivalent circuit models in the EIS analysis provided insights into the surface structure and behavior of the coatings.

Overall, the incorporation of BG into TC4 coatings showed potential for enhancing the bioactivity of the coatings while preserving their electrochemical corrosion-resistance properties. Further investigations are warranted to explore the bioactivity aspects and potential biomedical applications of TC4/BG composite coatings.

Author Contributions: Conceptualization, Y.Y., C.Z., X.C. and P.S.; Funding acquisition, Y.Y. and X.C.; Investigation, Y.M. and J.K.; Methodology, Y.Y. and E.L.; Project administration, Y.Y. and X.C.; Supervision, Y.Y.; Validation, Y.M. and G.J.; Writing—original draft, Y.M. and Y.Y.; Writing—review and editing, Y.M., Y.Y. and E.L. All authors have read and agreed to the published version of the manuscript.

Funding: The research was funded by National Natural Science Foundation of China (No. 52205189 and 51975137) and supported by Heilongjiang Provincial Natural Science Foundation of China (LH2020E063).

Institutional Review Board Statement: Not applicable.

Informed Consent Statement: Not applicable.

Data Availability Statement: Data is contained within the article.

Conflicts of Interest: The authors declare no conflict of interest.

Abbreviations

Bioactive glass	(BG)
Charge transfer resistance of the dense barrier layer	(R_b)
Charge transfer resistance of the porous layer	(R_p)
Constant phase angle element	(CPE)
Constant phase angle element of the dense barrier layer	(Q_b)
Constant phase angle element of the porous layer	(Q_p)
Corrosion current density	(I_{corr})
Dulbecco's modified Eagle medium	(DMEM)
Electrochemical impedance spectroscopy	(EIS)
Electrolyte resistance	(R_s)
Heat-affected zone	(HAZ)
Open circuit potential	(OCP)
Passivation current density	(I_{pp})
Scanning electron microscopy	(SEM)
Solidification rate	(R)
Temperature gradient	(G)
Ti-6Al-4V	(TC4)
X-ray diffraction	(XRD)

References

1. Alabort, E.; Barba, D.; Shagiev, M.R.; Murzinova, M.A.; Galeyev, R.M.; Valiakhmetov, O.R.; Aletdinov, A.F.; Reed, R.C. Alloys-by-Design: Application to Titanium Alloys for Optimal Superplasticity. *Acta Mater.* **2019**, *178*, 275–287. [CrossRef]
2. Liu, Z.; He, B.; Lyu, T.; Zou, Y. A Review on Additive Manufacturing of Titanium Alloys for Aerospace Applications: Directed Energy Deposition and Beyond Ti-6Al-4V. *JOM* **2021**, *73*, 1804–1818. [CrossRef]
3. Niinomi, M. Design and Development of Metallic Biomaterials with Biological and Mechanical Biocompatibility. *J. Biomed. Mater. Res. Part A* **2019**, *107*, 944–954. [CrossRef] [PubMed]
4. Chen, Q.; Thouas, G.A. Metallic Implant Biomaterials. *Mater. Sci. Eng. R Rep.* **2015**, *87*, 1–57. [CrossRef]
5. Jiang, P.F.; Nie, M.H.; Teng, J.Z.; Wang, X.B.; Liu, C.Z.; Zhang, Z.H. Multi-Wire Arc Additive Manufacturing of TC4/Nb Bionic Layered Heterogeneous Alloy: Microstructure Evolution and Mechanical Properties. *Mater. Sci. Eng. A* **2023**, *874*, 145076. [CrossRef]
6. Kurup, A.; Dhatrak, P.; Khasnis, N. Surface Modification Techniques of Titanium and Titanium Alloys for Biomedical Dental Applications: A Review. *Mater. Today Proc.* **2021**, *39*, 84–90. [CrossRef]
7. Bao, Y.; Wang, W.; Cui, W.; Qin, G. Corrosion Resistance and Antibacterial Activity of Ti-N-O Coatings Deposited on Dental Titanium Alloy. *Surf. Coat. Technol.* **2021**, *419*, 127296. [CrossRef]
8. Wang, J.; Pan, Y.; Feng, R.; Cui, H.; Gong, B.; Zhang, L.; Gao, Z.; Cui, X.; Zhang, H.; Jia, Z. Effect of Electrolyte Composition on the Microstructure and Bio-Corrosion Behavior of Micro-Arc Oxidized Coatings on Biomedical Ti6Al4V Alloy. *J. Mater. Res. Technol.* **2020**, *9*, 1477–1490. [CrossRef]
9. Han, X.; Ma, J.; Tian, A.; Wang, Y.; Li, Y.; Dong, B.; Tong, X.; Ma, X. Surface Modification Techniques of Titanium and Titanium Alloys for Biomedical Orthopaedics Applications: A Review. *Colloids Surf. B Biointerfaces* **2023**, *227*, 113339. [CrossRef]
10. Raut, H.K.; Das, R.; Liu, Z.; Liu, X.; Ramakrishna, S. Biocompatibility of Biomaterials for Tissue Regeneration or Replacement. *Biotechnol. J.* **2020**, *15*, 2000160. [CrossRef]

11. Wang, C.; Wang, Y.; Bao, Z.; Dong, J.; Geng, Y.; Liu, S.; Wang, C.; Nie, P. Characterization of Microstructure and Mechanical Properties of Titanium -Based Bioactive Ceramics Laser-Deposited on Titanium Alloy. *Ceram. Int.* **2022**, *48*, 28678–28691. [CrossRef]
12. Wu, B.; Xiong, S.; Guo, Y.; Chen, Y.; Huang, P.; Yang, B. Tooth-Colored Bioactive Titanium Alloy Prepared with Anodic Oxidation Method for Dental Implant Application. *Mater. Lett.* **2019**, *248*, 134–137. [CrossRef]
13. Muthaiah, V.M.S.; Indrakumar, S.; Suwas, S.; Chatterjee, K. Surface Engineering of Additively Manufactured Titanium Alloys for Enhanced Clinical Performance of Biomedical Implants: A Review of Recent Developments. *Bioprinting* **2022**, *25*, e00180. [CrossRef]
14. Sivaranjani, S.; Anusha Thampi, V.V.; Shalini, M.; Krishnakumar, G.S.; Veerapandian, M.; Shtansky, D.; Subramanian, B. Imparting Bioactivity to CP−Titanium with Sputtered TiBN Interlayer and Electrophoretically Grown Bioglass Overlay. *Mater. Chem. Phys.* **2023**, *298*, 127420. [CrossRef]
15. Deng, C.; Wang, Y.; Zhang, Y.; Gao, J. In Situ Laser Coating of Calcium Phosphate on TC4 Surface for Enhancing Bioactivity. *J. Iron Steel Res. Int.* **2007**, *14*, 73–78. [CrossRef]
16. Leilei, Z.; Hejun, L.; Kezhi, L.; Shouyang, Z.; Qiangang, F.; Yulei, Z.; Shoujie, L. Double-Layer TC4/Sr Substituted Hydroxyapatite Bioactive Coating for Carbon/Carbon Composites. *Ceram. Int.* **2015**, *41*, 427–435. [CrossRef]
17. Li, R.; Ying, B.; Wei, Y.; Xing, H.; Qin, Y.; Li, D. Comparative Evaluation of Sr-Incorporated Calcium Phosphate and Calcium Silicate as Bioactive Osteogenesis Coating Orthopedics Applications. *Colloids Surf. A Physicochem. Eng. Asp.* **2020**, *600*, 124834. [CrossRef]
18. Zeimaran, E.; Pourshahrestani, S.; Fathi, A.; bin Razak, N.A.A.; Kadri, N.A.; Sheikhi, A.; Baino, F. Advances in Bioactive Glass-Containing Injectable Hydrogel Biomaterials for Tissue Regeneration. *Acta Biomater.* **2021**, *136*, 1–36. [CrossRef]
19. Simila, H.O.; Boccaccini, A.R. Sol-Gel Bioactive Glass Containing Biomaterials for Restorative Dentistry: A Review. *Dent. Mater.* **2022**, *38*, 725–747. [CrossRef]
20. Patel, K.D.; Buitrago, J.O.; Parthiban, S.P.; Lee, J.-H.; Singh, R.K.; Knowles, J.C.; Kim, H.-W. Combined Effects of Nanoroughness and Ions Produced by Electrodeposition of Mesoporous Bioglass Nanoparticle for Bone Regeneration. *ACS Appl. Bio Mater.* **2019**, *2*, 5190–5203. [CrossRef]
21. Patel, K.D.; El-Fiqi, A.; Lee, H.-Y.K.; Singh, R.; Kim, D.-A.; Lee, H.-H.; Kim, H.-K. Chitosan–Nanobioactive Glass Electrophoretic Coatings with Bone Regenerative and Drug Delivering Potential. *J. Mater. Chem.* **2012**, *22*, 24945–24956. [CrossRef]
22. Yang, Y.; Zheng, K.; Liang, R.; Mainka, A.; Taccardi, N.; Roether, J.A.; Detsch, R.; Goldmann, W.H.; Virtanen, S.; Boccaccini, A.R. Cu-Releasing Bioactive Glass/Polycaprolactone Coating on Mg with Antibacterial and Anticorrosive Properties for Bone Tissue Engineering. *Biomed. Mater.* **2017**, *13*, 015001. [CrossRef] [PubMed]
23. Zheng, K.; Lu, M.; Rutkowski, B.; Dai, X.; Yang, Y.; Taccardi, N.; Stachewicz, U.; Czyrska-Filemonowicz, A.; Hüser, N.; Boccaccini, A.R. ZnO Quantum Dots Modified Bioactive Glass Nanoparticles with PH-Sensitive Release of Zn Ions, Fluorescence, Antibacterial and Osteogenic Properties. *J. Mater. Chem. B* **2016**, *4*, 7936–7949. [CrossRef] [PubMed]
24. Liu, Y.; Li, J.; Xu, Q.; Zhang, Y.; Yan, X.; Chen, Y.; He, H. Microstructure and Wear Behavior of TC4 Laser Cladding Modified via SiC and MoS2. *Coatings* **2022**, *12*, 792. [CrossRef]
25. Wan, S.; Cui, X.; Jin, G.; Ma, J.; Yang, Y.; Liu, K.; Li, J.; Wang, S.; Wang, J. Microstructure and Properties Characterization of Laser-Cladded CuAl Alloy Coatings on MgLi Alloy. *Surf. Coat. Technol.* **2023**, *460*, 129430. [CrossRef]
26. Zhao, H.; Yu, C.; Liu, Z.; Liu, C.; Zhan, Y. A Novel Finite Element Method for Simulating Residual Stress of TC4 Alloy Produced by Laser Additive Manufacturing. *Opt. Laser Technol.* **2023**, *157*, 108765. [CrossRef]
27. Ma, J.; Wang, C.Z.; Ban, C.L.; Chen, C.Z.; Zhang, H.M. Pulsed Laser Deposition of Magnesium-Containing Bioactive Glass Film on Porous Ti–6Al–4V Substrate Pretreated by Micro-Arc Oxidation. *Vacuum* **2016**, *125*, 48–55. [CrossRef]
28. Laser Cladding and Laser Direct Glass Deposition of Bioactive Glass and Glass-Ceramics—Bioactive Glasses and Glass-Ceramics: Fundamentals and Applications—Wiley Online Library. Available online: https://onlinelibrary.wiley.com/doi/abs/10.1002/9781119724193.ch14 (accessed on 22 July 2023).
29. Gu, H.; Zhang, G.; Cai, E.; Tang, G.; Liu, Q. Bioactivity and Biocompatibility of Porous Gradient Bioceramic Coating Prepared via Laser Cladding Process. *Surf. Coat. Technol.* **2021**, *426*, 127800. [CrossRef]
30. Ghaebi Panah, N.; Atkin, R.; Sercombe, T.B. Bioactivity and Biodegradability of High Temperature Sintered 58S Ceramics. *J. Eur. Ceram. Soc.* **2022**, *42*, 3614–3623. [CrossRef]
31. Huang, Y.; Zeng, X.; Hu, Q.; Zhou, S. Microstructure and Interface Interaction in Laser Induction Hybrid Cladding of Ni-Based Coating. *Appl. Surf. Sci.* **2009**, *255*, 3940–3945. [CrossRef]
32. Zhou, Z.; Li, H.; Liu, Y.; Niu, T.; Li, H. Effect of Ti on the Corrosion Behavior of (FeCrCoNi)100−xTix Alloy. *Corros. Sci.* **2022**, *209*, 110807. [CrossRef]
33. Ji, P.F.; Li, B.; Chen, B.H.; Wang, F.; Ma, W.; Zhang, X.Y.; Ma, M.Z.; Liu, R.P. Effect of Nb Addition on the Stability and Biological Corrosion Resistance of Ti-Zr Alloy Passivation Films. *Corros. Sci.* **2020**, *170*, 108696. [CrossRef]
34. Radu, M.M.; Becherescu, N.; Spătaru, T.; Osiceanu, P.; Mihai, M.A.; Calderon-Moreno, J.M.; Spătaru, N.; Fujishima, A. Improved Suitability as Catalyst Support and More Efficient Charge Carrier Separation of Native Air-Formed TiO_2 Films by Mild Laser Treatment. *J. Power Sources* **2019**, *437*, 226921. [CrossRef]

35. Spataru, T.; Mihai, M.A.; Preda, L.; Marcu, M.; Radu, M.M.; Becherescu, N.D.; Velea, A.; Zaki, M.Y.; Udrea, R.; Satulu, V.; et al. Enhanced Photoelectrochemical Activity of WO3-Decorated Native Titania Films by Mild Laser Treatment. *Appl. Surf. Sci.* **2022**, *596*, 153682. [CrossRef]
36. Khan, M.A.; Williams, R.L.; Williams, D.F. The Corrosion Behaviour of Ti–6Al–4V, Ti–6Al–7Nb and Ti–13Nb–13Zr in Protein Solutions. *Biomaterials* **1999**, *20*, 631–637. [CrossRef] [PubMed]
37. Li, Z.; Wang, J.; Dong, Y.; Xu, D.; Zhang, X.; Wu, J.; Gu, T.; Wang, F. Synergistic Effect of Chloride Ion and Shewanella Algae Accelerates the Corrosion of Ti-6Al-4V Alloy. *J. Mater. Sci. Technol.* **2021**, *71*, 177–185. [CrossRef]
38. Fekry, A.M. The Influence of Chloride and Sulphate Ions on the Corrosion Behavior of Ti and Ti-6Al-4V Alloy in Oxalic Acid. *Electrochim. Acta* **2009**, *54*, 3480–3489. [CrossRef]
39. Bai, C.; Li, P.; Gang, T.; Li, J.; Wei, M.; Huang, Y.; Chen, L. Influence of Processing Technology on Electrochemical Corrosion Behavior of Ti-6Al-4V Alloys. *Corrosion* **2021**, *77*, 402–412. [CrossRef]
40. Mehdipour, M.; Afshar, A.; Mohebali, M. Electrophoretic Deposition of Bioactive Glass Coating on 316L Stainless Steel and Electrochemical Behavior Study. *Appl. Surf. Sci.* **2012**, *258*, 9832–9839. [CrossRef]
41. de Assis, S.L.; Wolynec, S.; Costa, I. Corrosion Characterization of Titanium Alloys by Electrochemical Techniques. *Electrochim. Acta* **2006**, *51*, 1815–1819. [CrossRef]
42. Bins-Ely, L.; Cesca, K.; Souza, F.S.; Porto, L.; Spinelli, A.; Magini, R.; Henriques, B.; Souza, J.C.M. On the Increase of the Chemical Reactivity of Cp Titanium and Ti6Al4V at Low Electrical Current in a Protein-Rich Medium. *Biomed. Phys. Eng. Express* **2018**, *5*, 015014. [CrossRef]
43. Monticelli, C.; Zucchi, F.; Tampieri, A. Triboelectrochemical Behaviour of a Si3N4–TiN Ceramic Composite and a Titanium Alloy Commonly Used in Biomedical Applications. *Wear* **2009**, *266*, 327–336. [CrossRef]
44. Guo, S.; Lu, Y.; Wu, S.; Liu, L.; He, M.; Zhao, C.; Gan, Y.; Lin, J.; Luo, J.; Xu, X.; et al. Preliminary Study on the Corrosion Resistance, Antibacterial Activity and Cytotoxicity of Selective-Laser-Melted Ti6Al4V-XCu Alloys. *Mater. Sci. Eng. C* **2017**, *72*, 631–640. [CrossRef]
45. Wang, Z.B.; Hu, H.X.; Liu, C.B.; Zheng, Y.G. The Effect of Fluoride Ions on the Corrosion Behavior of Pure Titanium in 0.05M Sulfuric Acid. *Electrochim. Acta* **2014**, *135*, 526–535. [CrossRef]
46. Tamilselvi, S.; Raman, V.; Rajendran, N. Corrosion Behaviour of Ti–6Al–7Nb and Ti–6Al–4V ELI Alloys in the Simulated Body Fluid Solution by Electrochemical Impedance Spectroscopy. *Electrochim. Acta* **2006**, *52*, 839–846. [CrossRef]

Disclaimer/Publisher's Note: The statements, opinions and data contained in all publications are solely those of the individual author(s) and contributor(s) and not of MDPI and/or the editor(s). MDPI and/or the editor(s) disclaim responsibility for any injury to people or property resulting from any ideas, methods, instructions or products referred to in the content.